Environmental Effects on the Spectroscopic Properties of Gallic Acid: A Combined Classical and Quantum Mechanical Study

Chiara Cappelli,*,† Benedetta Mennucci,‡ and Susanna Monti§

PolyLab-INFM, c/o Dipartimento di Chimica e Chimica Industriale, Università di Pisa, via Risorgimento 35, I-56126 Pisa, Italy, Dipartimento di Chimica e Chimica Industriale, Università di Pisa, via Risorgimento 35, I-56126 Pisa, Italy, and Istituto per i Processi Chimico-Fisici (IPCF-CNR), Area della Ricerca, via G. Moruzzi 1, I-56124 Pisa, Italy

Received: November 15, 2004; In Final Form: December 23, 2004

The solvation of gallic acid (in water and acetonitrile) is studied by means of its spectroscopic properties. IR, UV, and NMR spectra are predicted by using various solvation models obtained in terms of both purely classical and density functional approaches. Comparison with experiments is used to validate solvation models. Hydrogen-bond and long-range (or bulk) effects are evaluated by comparing different solvation models. A continuum-only approach, a purely discrete, and a mixed continuum/discrete approach based on quantum-mechanical and classical molecular-dynamics solute−solvent clusters are tested.

1. Introduction

Gallic acid (GA, 3,4,5-trihydroxybenzoic acid) can be considered the simplest prototype of vegetable tannins, a class of natural polyphenolic compounds extracted from plants and significantly present in human diets, whose chemical and biochemical properties have been evidenced.[1−4] Polyphenolic compounds are involved in many metabolic reactions and are widely used as antioxidant food additives:[5] gallic acid itself is a strong natural antioxidant commonly found in a wide variety of foodstuffs and beverages such as tea and wine. Numerous studies have demonstrated that polyphenolic compounds have anti-inflammatory, antimutagenic, antibacterial, antiviral, and immune-stimulating properties, and the main mechanism proposed for their protective action has been related to their free radical scavenging activity. There is more and more proof indicating that they could be used as drugs in the prevention of pathologies such as cancer (for their antiproliferative and cytotoxic qualities), cardiovascular diseases, and inflammatory disorders.[2,6] In particular, gallic acid is a strong chelating,[7] phytotoxic, and antifungal agent[8] and has been shown to be effective in atherosclerosis prevention.[9]

Polyphenols also show a wide and contradictory behavior involving a variety of harmful effects on animals and humans.[10] Indeed, they can affect negatively the utilization of vitamins and minerals,[11] and they can inhibit digestive enzymes and act as second-stage tumor promoters.[12] Besides their biochemical and biological interest, polyphenolic compounds are also used in the leather industry, in the processing of vegetable tanning. This process involves the binding of polyphenols with collagen.[13,14] The same binding property has recently been exploited to develop an optical sensor based on FTIR spectroscopy.[15]

It has been shown that the activity of polyphenolic compounds depends on their structural characteristics.[2,16] Thus, the investigation of the structure and spectroscopic properties of such molecules can hopefully lead to a better understanding, at the molecular level, of their biochemical structure−activity relationships. So far, however, the conformational and spectral properties of these systems have received only little attention; to the best of our knowledge, only a few studies on molecular orbital calculations on polyphenolic acids derivatives are present in the literature.[6,17,18] Even less investigated are the spectroscopic properties of gallic acid, being the subject of only two recent papers:[3,18] one concerning the modification of absorbance and fluorescence with the ionization state in aqueous and micellar environment[3] and the other dealing with vibrational spectra of gallic acid in the gas phase.[18]

Here, for the first time, conformational and spectroscopic properties of gallic acid in the gas phase and in polar solvents are studied using a combination of molecular mechanics (MM), molecular dynamics (MD), and quantum mechanics (QM) calculations. Such a study is divided in two steps. First, the potential energy surface (PES) of gallic acid is explored and the minimum energy structures are identified both in the gas phase and in solution. Then, the effects due to the environment on infrared (IR), electronic absorption (UV), and nuclear magnetic resonance (NMR) spectra are interpreted in terms of various solvation models, ranging from a purely continuum one to mixed continuum-discrete solvation approaches. The results of the various models are finally compared so to predict and rationalize spectroscopic properties of gallic acid in aqueous and acetonitrile solution.

The continuum solvation model which will be used here is the so-called integral equation formalism (IEF),[19] the most recent development of the largely diffused polarizable continuum model (PCM) method.[20] This is an accurate continuum solvation model which uses a molecular-shaped cavity to define the boundary between solute and continuum dielectric and apparent surface charges to describe the electrostatic solvent effects. In the past few years, this model has been extended to evaluate solvent effects on molecular properties.[21] The discrete model used here exploits two approaches. In the first approach, small clusters (the solute plus few H-bonded water molecules) are obtained through ab initio geometry optimizations. This ap-

* Corresponding author. E-mail: chiara@dcci.unipi.it.
† PolyLab-INFM.
‡ Università di Pisa.
§ IPCF-CNR.

10.1021/jp044781s CCC: $30.25
Published on Web 02/10/2005

proach has been successfully coupled to IEFPCM in previous papers to study various molecular properties.[22−24] In the second approach, solute−solvent clusters are obtained from molecular dynamics (MD) runs by defining a proper solvation shell radius.[25]

2. Computational Details

2.1. Quantum-Mechanical Calculations. All QM calculations were performed with the Gaussian 03 computational code[26] using the Becke three parameter Lee−Yang−Parr functional (B3LYP) and the 6-311++G** basis set. Solvent effects were introduced through a continuum, a discrete model in terms of solute−solvent clusters, or with the combination of the two approaches in terms of "solvated" clusters (e.g., solute−solvent clusters with the addition of an external continuum).

The integral equation formalism (IEF)[19] version of the polarizable continuum model (PCM)[20] was used as continuum solvation model. The molecular cavity was obtained in terms of interlocking spheres centered on carbons, oxygens, and hydroxylic and phenolic hydrogens. The radius of each sphere was obtained by scaling the corresponding van der Waals radius by a factor of 1.2, thus obtaining the following R(C) = 2.04 Å, R(CH) = 2.28 Å, R(O) = 1.824 Å, R(H) = 1.44 Å.[27]

Two sets of solute−solvent clusters were exploited. One set was obtained from MD runs (see below). The second set was generated by optimizing at B3LYP/6-311++G** GA with one, two, and eight water molecules H-bonded to carboxylic and phenolic groups. The structures of both GA and QM clusters were obtained both in gas-phase and with the IEFPCM continuum.

IR spectra in solution were simulated by taking into account cavity field effects according to the model reported in ref 28. The first few singlet excitation energies of GA were calculated at the density functional level using the time dependent perturbation theory approach (TDDFT); the IEFPCM excitation energies were obtained within the nonequilibrium solvation scheme.[29] NMR nuclear shieldings were computed by using the Gauge-including atomic orbitals (GIAO):[30] the inclusion of solvent effects within this formalism has been presented in ref 31. NMRPCM For all clusters basis-set-superposition errors were eliminated by using the Counter-Poise (CP) approach.[32]

2.2. Conformational Analysis. To identify the relevant conformers of GA a systematic conformational search of the potential energy surface (PES) was carried out using MMFF94 force field[33] and charge model in SYBYL[34] with a dielectric constant $\epsilon = 1$. The conformations were generated by rotating τ_1, τ_2, τ_3, τ_4 and τ_5 dihedral angles from 0 to 180° by 30° increments (see Figure 1).

Each structure obtained in this way was optimized and its energy was computed. Conformations with energies greater than 32 kcal/mol above the lowest energy structure were rejected and the remaining geometries were analyzed. The relative stability of the 16 selected conformers was computed with molecular mechanics (MMFF94 and AMBER GAFF[35]) and density functional (B3LYP/6-311++G** in the gas phase and in water) methods.

In Figure 2a, the correlation between the MMFF94 relative energies at its own minimum and those determined with B3LYP/6-311++G** in vacuo, with B3LYP/6-311++G** in water (e.g., with the IEFPCM), and with the AMBER GAFF force field are reported.

The B3LYP/6-311++G** results in the gas phase correlate satisfactorily with the MMFF94 ones ($R = 0.953$), whereas the correlation coefficient between B3LYP/6-311++G** in water and MMFF94 is slightly worse ($R = 0.898$). As far as the AMBER GAFF force field is concerned, it compares fairly well with MMFF94 ($R = 0.986$).

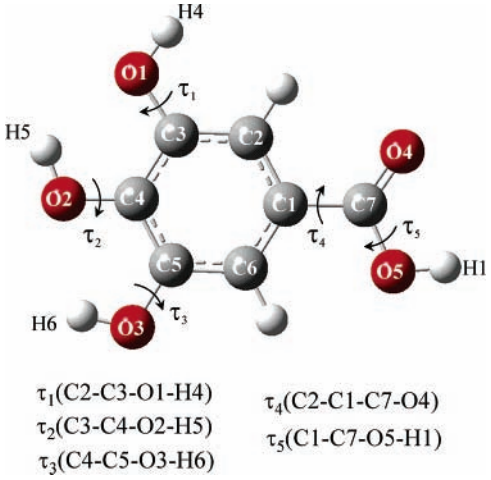

Figure 1. Atom numbering of GA and definition of the torsional angles.

In Figure 2b, the correlation between the AMBER GAFF relative energies at its own minimum and those determined with B3LYP/6-311++G** in vacuo, B3LYP/6-311++G** in water, and MMFF94 are reported.

As it can be seen, AMBER GAFF correlates decidedly better than MMFF94 with the B3LYP/6-311++G** results both in the gas phase and in water with correlation coefficients $R = 0.985$ and 0.959, respectively. However, all of the methods agree in identifying the first and the second most stable conformers.

Among the 16 selected structures, the two most stable both in gas-phase and in water are those with $\tau_i = 0$ ($i = 1-4$) and $\tau_5 = 180$ (structure A) and with $\tau_i = 0$ ($i = 1-3$) and $\tau_i = 180°$ ($i = 4$ and 5) (structure B). The B3LYP/6-311++G** free energy difference between A and B is −0.350 kcal/mol in gas-phase and −0.059 in water (these data include zero-point energy, ZPE, and thermal corrections at 298 K). All the other conformations differ from the first two most stable structures by more than 3.0 kcal/mol in gas-phase and 1.0 kcal/mol in water; these differences imply Boltzmann factors of the order of 5×10^{-3} in gas-phase and 5×10^{-2} in water, and thus, they can be neglected in the following analysis. We note that the minimum energy structures A and B here found in gas-phase and in aqueous solution are different from that proposed in a previous study by Mohammed-Ziegler and Billes[18] where however a conformational analysis as that performed here was not reported.

2.3. Molecular Dynamics Simulations. Following the previous analysis, GA lowest energy geometry (structure A) was chosen for MD simulations in solution. MD simulations were performed with AMBER7 software[35] in aqueous and acetonitrile solution using an explicit representation of solvent molecules. The TIP3P model[36] was used for water molecules, whereas the acetonitrile solvent was modeled according to Grabuleda et al.[37] with an all atom solvent model whose density, heat of vaporization, and isothermal compressibility values are in good agreement with available experimental data especially for a generic force field such as the AMBER-GAFF one. Parameters for GA were taken from the gaff force field and from previous studies of ours.[14]

The partial charges were obtained from a 6-311++G** density functional theory calculation with the B3LYP functional

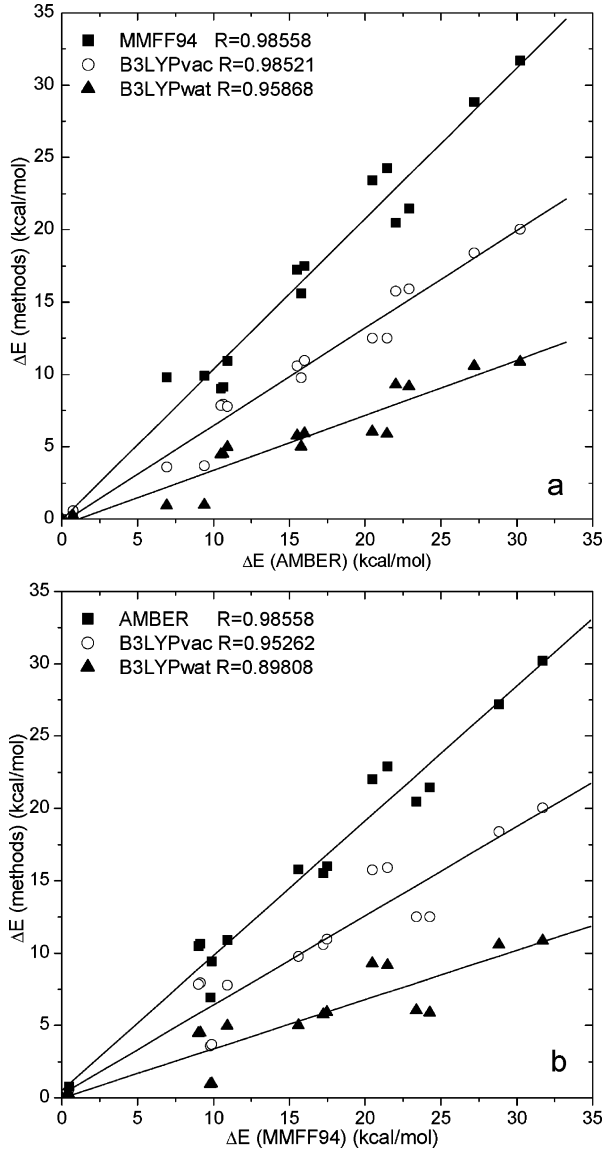

Figure 2. Correlation between the MMFF94 relative energies at its own minimum and those determined with B3LYP/6-311++G** in vacuo, B3LYP/6-311++G** in water (e.g., with the IEFPCM) with AMBER GAFF force field (a); and between AMBER GAFF and B3LYP/6-311++G** in vacuo, B3LYP/6-311++G** in water (e.g., with the IEFPCM) with MMFF94 (b).

in the equilibrium geometry employing the RESP procedure;[38] the effects of a continuum model (see above) were also included.

A residue based 12 Å cutoff was applied to the nonbonded interactions using three-dimensional periodic boundary conditions. A particle mesh Ewald (PME) correction to the long-range electrostatics was applied. All MD simulations were performed at constant pressure (1 atm) and at a temperature maintained at 298 K by coupling the system to a thermal bath using Berendsen algorithm,[39] and the integration time step was set to 1 fs. The equilibration procedure was done in two steps: a solvent position randomization phase during which the system was heated under constant volume conditions to 500 K over 5 ps of dynamics while keeping fixed the solute coordinates then cooled to 298 K over 10 ps and a real equilibration at constant pressure for a period sufficient to reach a reasonable density. About 15 ps were needed for total achievement of the equilibrium. Starting from the equilibrated system, MD trajectories were recorded for a maximum of 1 ns by freezing GA atom positions in order to characterize the water and acetonitrile cluster structures. The coordinates were saved every 0.1 ps to analyze the trajectories.

With the information supplied from the computed radial distribution functions (RDFs), some solute−solvent clusters were selected on the basis of a cutoff distance (r_{cut}) for the O−H and H−O pairs: each cluster included all solvent molecules having the hydrogen (oxygen) atom closer than r_{cut} to the solute oxygen (hydrogen). The value used for r_{cut} was 5 Å. With this criterion, sets of 100 structures were generated, with 10 ps being the separation between two consecutive structures. This large time distance avoids any kind of correlation in the structures selected, so a proper sampling can be performed based on the configurations used. This has been confirmed by comparing the RDFs resulting from the subsystems of selected structures with those of the whole group of 10 000 configurations. From these, 10 structures, which have been used in the analysis on the spectroscopic properties of GA in water solution, were randomly extracted.

3. Results and Discussion

3.1. MD Analysis. In this section, the results obtained from MD simulations of GA both in water and acetonitrile solutions are examined. For both solvents radial distribution functions together with an analysis on coordination numbers and residence times for the different solute−solvent interacting sites are reported.

3.1.1. Water. Our attention has been focused on the solute−solvent hydrogen bonding interactions that mainly involve the solvent molecules of the first solvation shell. To obtain information on the extent of solvent structure and to illustrate the hydrogen bonding behavior of GA hydroxyl and carbonyl groups, intermolecular RDFs OX(GA)···HW and HX(GA)···OW and the corresponding coordination numbers (CN) were calculated (see Figure 3, parts a and b, for oxygen RDF and CN, and Figure 3, parts c and d, for hydrogen RDF and CN). The RDFs describe the local density of the solvent at a distance *r* from the solute atoms relative to the bulk density and approach unity for large distances where the local density converges to its bulk value.

The O3(GA)···HW and O4(GA)···HW radial distribution functions (see Figure 3a) show a sharp peak for the first solvation shell with a maximum at a distance of 1.98 and 1.79 Å and coordination numbers of 1.1 and 2.0, respectively, and a second more diffuse peak at 3.35 and 3.12 Å with coordination numbers of 10.4 and 6.4, respectively (Figure 3b). The O1(GA)···HW, O2(GA)···HW, and O5(GA)···HW RDFs show a broad peak at higher distances in the second solvation shell (3.36, 3.54, and 3.38 Å with coordination numbers of 10.0, 9.0, and 15.6).

The H1(GA)···OW and H4(GA)···OW RDFs (Figure 3c) show a pronounced first narrow peak at about the same distance of 1.75 Å with a coordination number of 1.0 and a second peak at 3.94 Å and 3.81 Å with coordination numbers of 15.5 and 13.0, respectively (Figure 3d). A first peak at 1.98 Å with a coordination number of 0.9 and a second peak at about 3.77 and 3.47 Å with coordination numbers of 9.9 and 7.7 are observed for H5(GA)···OW and H6(GA)···OW RDFs.

The RDFs analyses indicate that during the whole MD simulation (1 ns) water approaches all GA "active sites" (those that may be involved in intermolecular hydrogen bonds) at a hydrogen bonding distance (2.5 Å). O1, O2, O5, H5, and H6 atoms are "poorly" solvated by water being engaged in intramolecular hydrogen bonds, whereas O3, O4, H1, and H4 atoms are more exposed and thus accessible to solvent mol-

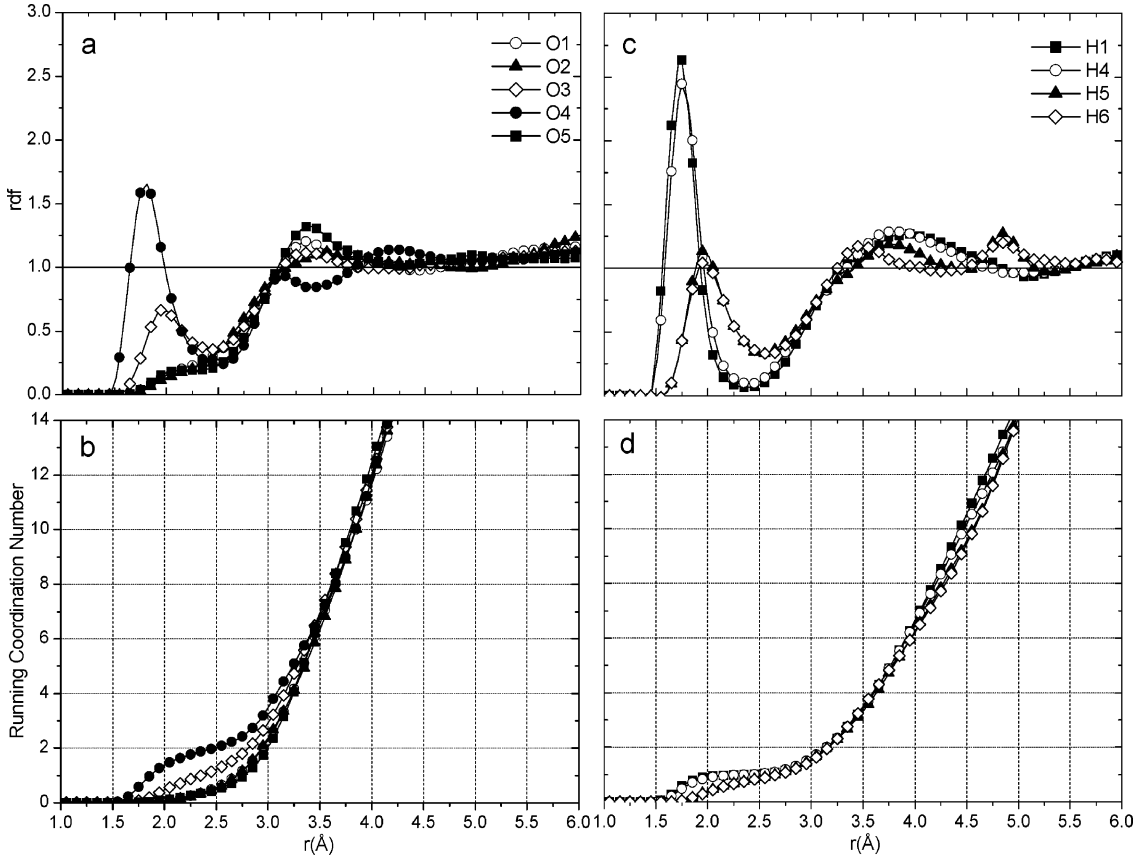

Figure 3. OX(GA)···HW and H(GA)···OW radial distribution functions (a and c) and coordination numbers (b and d).

TABLE 1: Water Residence Times (ps) around GA Oxygen Atoms[a]

		O1	O2	O3	O4	O5
0 WAT	min	1.1	1.5	3.2		4.5
	mean	46.4	50.9	7.0		28.4
	max	200.6	137.0	11.4		70.9
1 WAT	min	1.4	1.5	2.0	1.1	1.0
	mean	9.5	7.6	40.6	3.0	5.0
	max	34.3	17.8	96.4	8.1	17.0
2 WAT	min			1.3	4.5	
	mean			7.0	49.4	
	max			21.4	127.5	
3 WAT	min				1.8	
	mean				3.6	
	max				8.6	

[a] Four different cases are reported, namely the occurrence of zero (0 WAT), one (1 WAT), two (2 WAT), and three (3 WAT) water molecules. For each case, minimum (min), mean, and maximum (max) values are reported.

ecules. Water molecules exchange extensively between the first and the second shell and some of them diffuse also from far beyond this last one. The positive slope of all running coordination number plots (Figure 3, parts c and d) indicates solvent exchange between the shells. No horizontal plateaux are noticeable.

A series of solvent residence times were calculated by using the whole trajectory and averaged out to obtain a mean residence time. Such values were determined at GA oxygen sites to give a description of solvent mobility and the strength of the intermolecular interactions (Table 1).

Mean residence times (MRT) of water molecules around GA oxygen atoms were calculated considering only those solvent molecules within a distance of 2.5 Å which corresponds to the first minimum in the radial distribution functions. Any water molecule that returned to this coordination shell after escaping for less than 1 ps was considered to be continuously bound to the examined GA oxygen, whereas any molecule that was out of the coordination shell for longer than 1 ps was considered to be a free molecule. The residence time of 0, 1, 2, and 3 solvent molecules around each GA oxygen was defined as the duration of the time for which these molecules were bound to the considered site.

As can be seen, O3 and O4 are always surrounded by at least one water molecule, the 0-water MRT is zero for O4 and only 7.0 ps for O3. The 1-water O3 mean residence time together with the 2-water O4 mean residence time are the longest. This is not surprising as long as O3 and O4 are sites which are most exposed to the solvent. At the other end of the time scale, waters on O1, O2, and O5 have mean residence times lower than 10 ps and the 0-water mean residence times longer than 28 ps. These results well agree with the steric hindrance of each nucleus: O1 and O2, being the most hindered, present the highest 0-water MRT while O5 MRT is twice lower.

3.1.2. Acetonitrile. The HX(GA)···N_{MeCN} solvent RDFs are reported in Figure 4a.

H1(GA)···N_{MeCN} and H4(GA)···N_{MeCN} RDFs show a first narrow peak with the maximum at about 1.95 Å with a density of roughly 5 times the average bulk density. Integration of this first peak up to the first minimum at approximately 2.75 Å gives an average coordination number of 1.05 acetonitrile molecules. H5(GA)···N_{MeCN} and H6(GA)···N_{MeCN} RDFs have a first solvation shell peak centered at 2.15 Å with coordination number of 1.05 obtained by integration up to their first minimum at about 3.35 Å and a density of roughly 2 times the average bulk density.

From these data, it is evident that acetonitrile molecules equilibrate themselves closer to H1 and H4 (the most exposed

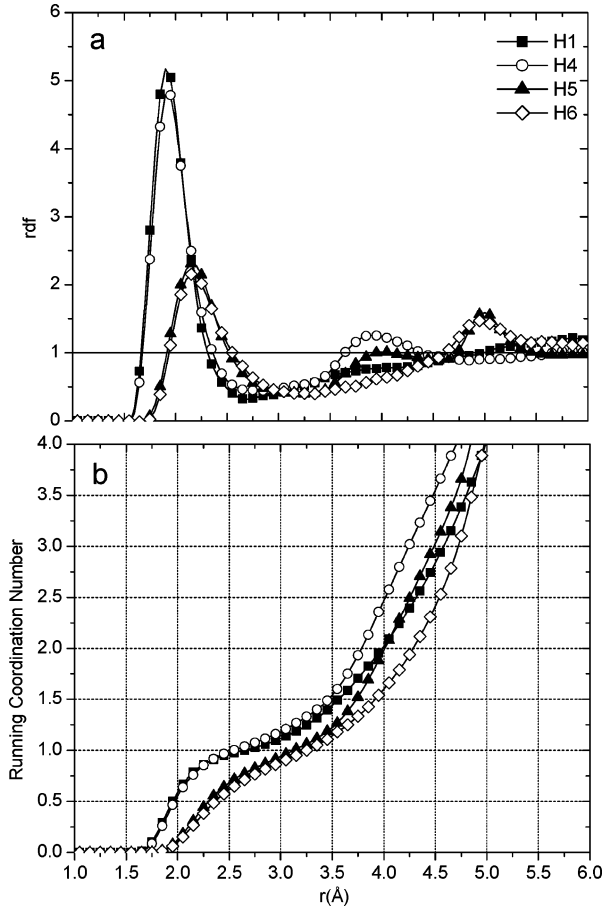

Figure 4. $HX(GA)\cdots N_{MeCN}$ radial distribution functions (a) and coordination numbers (b).

to solvent), whereas they are found at longer distances from H5 and H6 which are involved in intramolecular hydrogen bonds. All of the RDFs show a series of broad peaks at distances longer than 3.5 Å.

The running coordination numbers, plotted in Figure 4b, exhibit a positive slope which again indicates solvent exchange between the shells. An average number of 14 acetonitrile molecules is found in the first solvation shell during the whole simulation. Notice also that, with respect to the parallel plot for water (3d), here the CN for the 5 Å shell is 1/4 the value found for water.

Residence times of acetonitrile molecules around GA oxygen atoms were calculated considering only those solvent molecules within a distance of 3.0 Å (Table 2). Similarly to water, any acetonitrile molecule that returned to this coordination shell after escaping for less than 0.5 ps was considered to be continuously bound to the examined GA oxygen, whereas any molecule that was out of the coordination shell for longer than 0.5 ps was considered to be a free molecule.

O1, O2, O3, and O5 have the longest 1-MeCN mean residence time with a maximum of 16.0 ps for O1 whose hydrogen is more exposed to the solvent. O5 has the longest 3-MeCN mean residence time whereas O3 has the longest 2-MeCN mean residence time. Among the O4 mean residence times, the 0-MeCN is the longest.

The times that acetonitrile molecules spend near each GA oxygen before moving to other sites are shorter than those found for water molecules. There are no acetonitrile molecules that do not move at all, and a high exchange rate between sites and shells is observed. Most traffic involves also exchanging with the bulk. This rate is reduced for water due to the highest number

TABLE 2: Acetonitrile Residence Times (ps) around GA Oxygen Atoms[a]

		O1	O2	O3	O4	O5
0 MeCN	min	0.8	0.5	0.5	4.6	0.5
	mean	2.5	10.4	5.7	9.4	5.1
	max	4.1	34.3	19.6	14.3	18.6
1 MeCN	min	0.8	0.5	0.5	0.5	0.8
	mean	16.0	13.0	12.6	6.1	10.5
	max	53.4	67.2	41.7	22.1	36.2
2 MeCN	min	0.5	0.8	2.0	0.7	0.5
	mean	9.3	6.3	11.3	8.8	9.6
	max	41.7	17.6	35.3	35.6	48.2
3 MeCN	min	0.9		1.6	0.5	0.5
	mean	3.3		6.6	2.6	7.4
	max	8.6		8.4	11.7	25.4

[a] Four different cases are reported, namely the occurrence of zero (0 MeCN), one (1 MeCN), two (2 MeCN), and three (3 MeCN) acetonitrile molecules. For each case, minimum (min), mean, and maximum (max) values are reported.

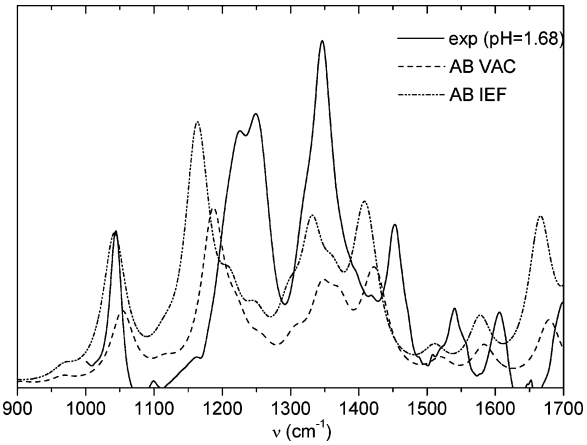

Figure 5. B3LYP/6-311++G** (gas and IEF) and experimental (in water at pH = 1.68) IR spectra of GA. The calculated spectra are obtained by averaging over the A and B conformers.

of interaction sites (both GA oxygen and hydrogen atoms) and to stronger hydrogen bonding interactions.

All these findings show that acetonitrile has not preferential interaction sites with GA and that its molecules rapidly exchange among shells. These two behaviors suggest a by far larger selectivity of water with respect to acetonitrile and that the effects of this latter on GA are of averaged (or "bulk") type.

3.2. IR Spectra in Water. To reproduce experimental IR spectra of GA in water, the two most stable conformations (the structures A and B introduced in section 2.2) have been considered, whose Boltzmann factors at 298 K are 0.644 and 0.356 in the gas-phase and 0.525 and 0.475 in water, respectively. These factors have been obtained from the free energies including zero-point and thermal corrections of the optimized B3LYP/6-311++G** A and B structures.

The resulting averaged spectra are reported in Figure 5 together with the experimental one measured at pH = 1.68. At this pH value, the observed spectrum can be considered as determined by the neutral form of GA only.

The comparison between calculated and experimental spectra shows that the portion of the spectrum in the range 1200−1500 cm^{-1} is badly reproduced (both frequencies and peak intensities) by the calculations, either in the absence or in the presence of the continuum dielectric. Further analysis of Figure 5 shows an improvement in the peaks intensities passing from vacuo to IEFPCM; nevertheless, the discrepancies between calculated (in water) and experimental data indicate that, at least in the case

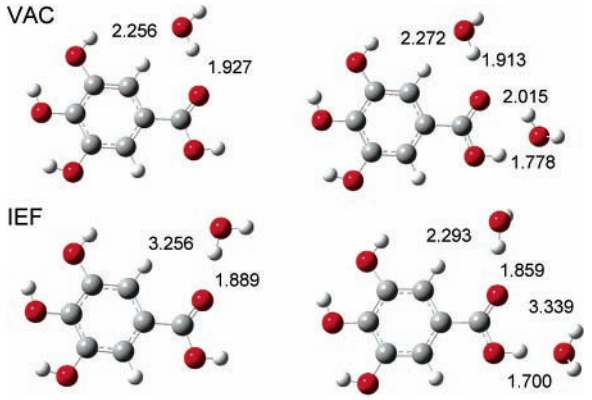

Figure 6. Graphical representation of A1w (left) and A2w (right) with the indication of selected interaction distances (in Å); the values refer to gas-phase optimization (upper panel) and to the IEF optimization (water, lower panel).

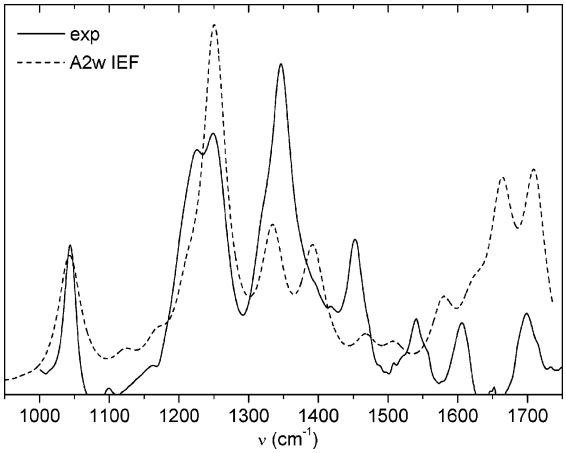

Figure 7. Comparison between B3LYP/6-311++G** IR spectrum of the A2w (including IEF continuum) cluster and experiments.

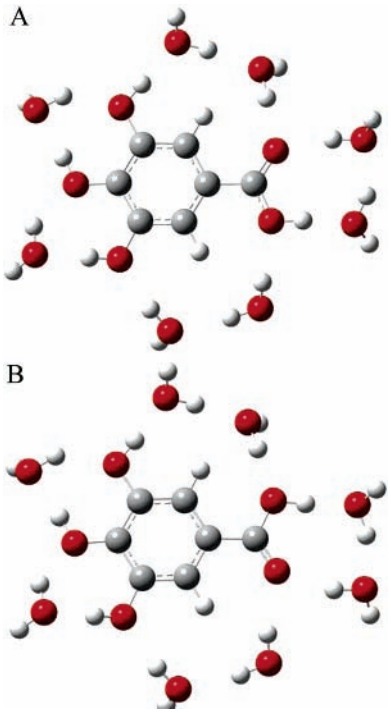

Figure 8. Graphical representation of A8w (top) and B8w (bottom) clusters.

of GA, the reduction of the effects of the aqueous environment to an average dielectric effect is not sufficient to explain the experimental behavior. For this reason, the description of the environment has been ameliorated by explicitly including specific first-shell hydrogen bonding effects. To this end, the information on the solvent structure around GA gained by means of MD simulations has been exploited and two different GA−water systems have been optimized at QM level (B3LYP/6-311++G**) with and without the IEF continuum.

As a first step, only two systems have been considered: in the first one (from now on indicated as A1w) a single water molecule hydrogen-bonded to the GA O4 atom is present; in the second one (which from now on is called A2w), the GA system bears two water molecules each involved in a single H-bonding with O4 and (O5)H.

As a further refinement in the model, the presence of the IEF continuum around the A1w and A2w structures has been considered. In Figure 6 the graphical representation of A1w (left) and A2w (right) with the indication of selected interaction distances is reported; the values refer to gas-phase optimization (upper panel) and to the IEF optimization (lower panel).

On these structures, IR spectra have been computed. We do not report here all the spectra, which can be found in the Supporting Information section, but we only note that little differences are found between the spectra of the A1w clusters and the averaged A + B spectra. As a result, the pure continuum approach seems to be able to well reproduce the solvent-induced polarization on the carbonyl group even in absence of the explicit consideration of first-shell effects. On the contrary, the A2w clusters lead to IR spectra markedly different from both the ones of the A1w clusters and that of the A + B system. In particular, a new intense band at about 1250 cm^{-1} appears, either when the continuum solvent is considered or not. The comparison between the spectrum of the A2w cluster and experimental findings[15] (Figure 7) shows an improvement in the overall description as a result of the introduction of the two water molecules. On the contrary, it appears that the explicit inclusion of hydrogen bond effects on the carboxylic groups does not affect the prediction of the intense band which is found in the experimental spectrum at about 1345 cm^{-1}. Notice that the intense band at around 1600 cm^{-1} in the calculated spectrum is due to water molecules and thus it cannot appear in the experimental spectrum, where such contribution has been subtracted.

To further investigate the nature of the intense experimental band at around 1345 cm^{-1} and in particular to connect the experimental findings to the microscopic solvated structure, additional calculations on the systems depicted in Figure 8 (from now on called A8w and B8w) have been performed: note that in this case, to obtain a complete description of the solvated system, both the A and B conformers of GA have been considered. Such structures model the GA system with all of the potential hydrogen bond sites saturated by water molecules. The calculations on the 8w clusters have been limited to the isolated systems, because in this case the solvent effect due to the explicit presence of the solvent molecules should reasonably be larger than the one due to the additional inclusion of the continuum environment.

The comparison between the averaged A8w+B8w spectrum and the experiment (see Figure 9) shows a clear improvement in the description. In particular, all of the peaks which are experimentally detected are now present in the calculated spectrum. The complex structure of the peaks at around 1250 and 1350 cm^{-1} is now reproduced very well and calculated intensities almost match experimental ones. The analysis of the

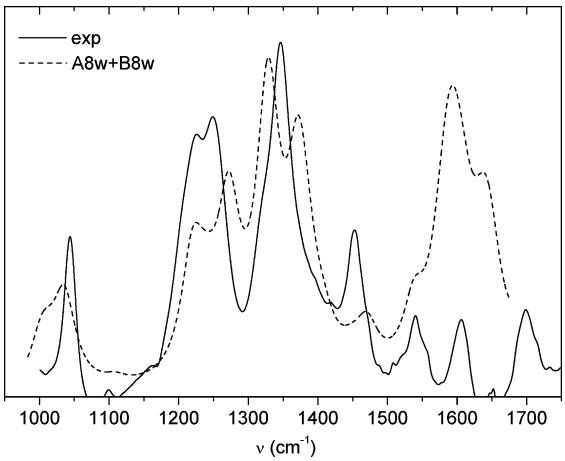

Figure 9. Comparison between B3LYP/6-311++G** averaged A8w+B8w IR spectrum and experiments.

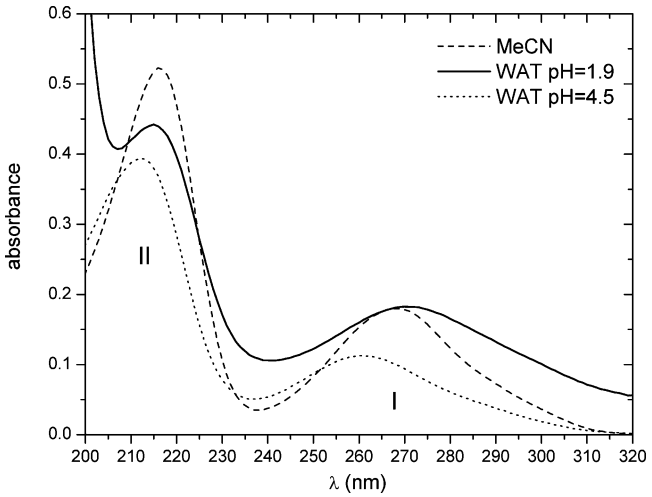

Figure 10. UV absorption spectrum of GA measured in two different solvents:[40] water (at pH = 1.9 and 4.5) and acetonitrile.

calculated frequencies of the 8w clusters shows an intense vibration at 1358 cm^{-1}, whose normal mode is composed of bending vibrations of the C−(phenolic)OH groups. In the case of GA (A or B structures), such a vibrations occurs at 1351 cm^{-1}, but its intensity is more than 7 times weaker than for the 8w clusters. In addition, in the A and B structures, the vibration at 1351 cm^{-1} is the weakest in the range 1300−1500 cm^{-1}, whereas in the case of the 8w clusters, the intensity of the mode at 1358 cm^{-1} is the largest between 1200 and 1600 cm^{-1}. This behavior can be due to the highest local asymmetry of the phenolic groups in the 8w clusters in comparison with A and B; the complex normal mode lying at 1358 cm^{-11} causes a distortion in the 8w structures which is greater than the corresponding ones in observed A and B (or equivalently 1w and 2w, where no water molecules are H-bonded to the phenolic groups). Such a greater distortion results in a larger variation in the molecular dipole moment, i.e., a greater infrared intensity.

3.3. UV Spectra. The electronic absorption spectrum of GA has been measured in two different solvents:[40] water (at pH = 1.9 and 4.5) and acetonitrile (Figure 10). Notice that here acetonitrile has also been considered because the comparison of the spectra in these two polar solvents permits to analyze solvation effects on GA into their bulk and H-bonding components.

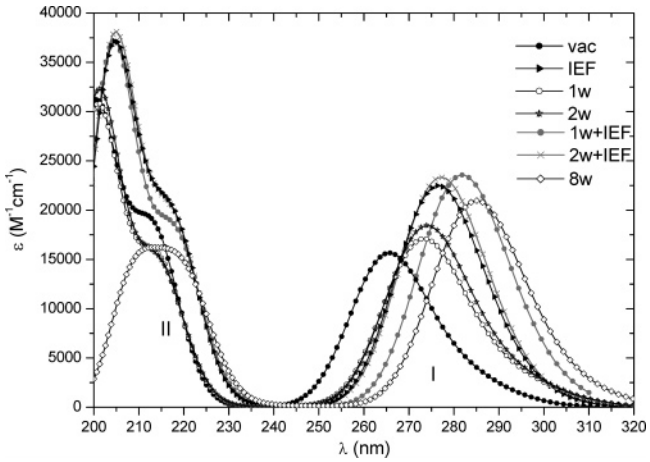

Figure 11. B3LYP/6-311++G** absorption spectra in gas-phase and in water (with various solvation models) obtained by summing oscillator strengths-weighted Gaussian curves with a full width at 1/e of the maximum of 0.15 eV for each calculated electronic transitions.

The spectra show a strong resemblance to each other having the same band structure with two well separated bands: I (240−310 nm) and II (205−230 nm).

The exact position of the two peaks depends on the ionization state of gallic acid molecules. In acidic solution, where gallic acid molecules are mostly neutral, the absorbance maxima are located at 270 and 215 nm; at pH = 4.5, the maxima shift to 260 and 212 nm respectively, due to the fact that in this case the carboxylic group is in the anionic form. The absorption maxima of the peaks in acetonitrile are red-shifted compared to those in water. The first maximum is shifted to 268 nm compared to 260 nm in water, whereas the shift of the second maximum is smaller (216 nm in acetonitrile compared to 212 nm in water).

The first few singlet excitation energies of GA have been calculated at the TDDFT level. The calculations have been performed in the gas phase, in acetonitrile and in water with IEFPCM.

Following the analysis of solvation given in section 3.1, which showed a by far larger selectivity of water with respect to acetonitrile, a continuum-only description for acetonitrile is used, whereas in the case of water, also in this section, clusters obtained by adding one, two, and eight explicit water molecules (eventually adding the external IEF continuum) are considered.

In Figure 11 theoretical simulated spectra, which have been obtained by summing oscillator strengths (*f*) weighted Gaussian curves with a full width at 1/e of the maximum of 0.15 eV for each calculated electronic transitions are compared.

In Table 3, the calculated vertical transitions, which have a clear correspondence to the two experimental distinct bands I and II, are reported. The lowest state yielding band I is a shorter wavelength excitation from the HOMO into the LUMO orbital (Figure 12), a π,π^* transition by which the band is dominated. Notice that the HOMO is a π type orbital mainly involving the aromatic ring while the LUMO π^* has important contributions from the carbonyl moiety. This excitation is located at 265 nm in the gas phase but it is red-shift in polar solutions to values that are in satisfactory agreement with the experimental data. It is interesting to analyze the effect of explicit water molecules and the bulk solvent effect computed by IEF.

To discuss these perturbations we will refer to the transition wavelength obtained in the gas phase. The influence of one or two explicit molecules hydrogen bonded to the carboxylic group on the π,π^* transition wavelength is a small red-shift of about

TABLE 3: Calculated (B3LYP/6-311++G) and Experimental Wavelengths for the Two Lowest π,π^* Transitions (Corresponding to Bands I and II) of GA Conformer A in Gas-Phase (vac), in Acetonitrile (MeCN), and in Water (wat)[a]**

	band	model	λ (nm)	f
vac	I		265	0.1986
	II		213	0.2293
MeCN	I	IEF	277	0.2799
	II	IEF	217	0.2416
wat	I	IEF	276	0.2775
		1w	273	0.2194
		2w	273	0.2369
		1w+IEF	281	0.2908
		2w+IEF	277	0.2888
		8w	284	0.2672
		$\langle md \rangle$	282	0.2878
wat	II	IEF	217	0.2420
		1w	214	0.1455
		2w	214	0.1797
		1w+IEF	218	0.2214
		2w+IEF	218	0.2361
		8w	219	0.1312
		$\langle md \rangle$	217	0.1626

[a] For solvated systems, the IEF model has been used, as well as QM (1w,2w,8w) and MD clusters ($\langle md \rangle$) possibly including the IEF continuum (nw+IEF). Calculated oscillatory strengths (f) are also reported. Experimental data are 268 and 216 nm for bands I and II in acetonitrile and 270 and 215 nm for bands I and II in water at pH = 1.9.[40]

8 nm ($\simeq$0.14 eV), whereas when considering the isolated GA molecule optimized in water described using the continuum approach, a much larger red-shift (11 nm, $\simeq$0.19 eV) is observed. On the other hand, by optimizing the clusters after the addition of the continuum, a substantial wavelength enlargement of the computed transition is obtained.

A complementary analysis can be done introducing clusters obtained from MD simulations (see section 2.3). The results reported in Table 3 for MD-derived systems refer to a set of 10 clusters selected as described above and used to compute band I without adding the IEF continuum. The computed energies of the different structures (which are not reported) of each set have been arithmetically averaged to give the values reported in Table 3 and marked as $\langle md \rangle$.

The $\langle md \rangle$ average result for band I is in line with the values computed including H-bond and bulk effects (see for example 1w+IEF).

This analysis appears to indicate that most of solvent effect is of pure electrostatic origin, in fact the main part of the gas-to-water shift is recovered by the continuum-only description and the additional inclusion of explicit waters only results in a further small correction. This is also shown by the results obtained for MD clusters when the water molecules are substituted by point charges (TIP3P): in this approximation a 13 nm shift with respect to isolated GA is obtained.

A larger red-shift (20 nm) occurs in the case of 8 explicit water molecules hydrogen bonded to all GA donor and acceptor atoms. This result indicates an overestimation of solvent effects in this cluster; if we consider that this band mainly involves the carbonyl moiety our results seem to suggest that the solvation introduced by this cluster overestimates H-bond effects on the carbonyl.

The highest energy π,π^* transition is the dominant contribution to the II band, which experimentally appears at (205−230 nm). It consists mainly of one single excitation from HOMO to LUMO+2 (in the gas phase and in water-IEF and in 1w+IEF), from HOMO to LUMO+3 (in 1w, 2w, and 2w+IEF), and from HOMO to LUMO+5 (8w), where LUMO+2, LUMO+3, and LUMO+5 are the same π^* orbital (refer to LUMO+n in Figure 12). This excitation is located at 215 ± 3 nm and no solvent effect on the wavelength position is found, in fact the HOMO−(LUMO+n) gap is nearly constant. This picture can be explained by looking at the orbitals involved in the transition, both are mainly centered on the aromatic ring and thus the effect of a polar (and eventually protic) solvent should reasonably be small.

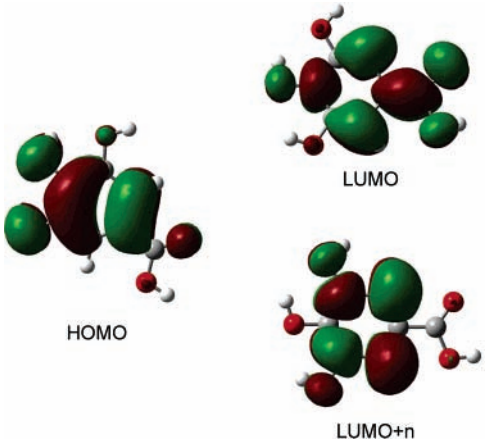

Figure 12. Occupied (HOMO) and virtual orbitals (LUMO,LUMO+n) involved in the π,π^* transitions studied.

TABLE 4: B3LYP/6-311++G (GIAO) ^{17}O Nuclear Shieldings (ppm) of GA A Conformer in Gas-Phase and in Solution[a]**

	vac	MeCN		water	
	σ	σ	δ	σ	δ
O1	233.03	231.50	−1.53	231.53	−1.50
O2	243.35	240.68	−2.67	240.86	−2.49
O3	225.50	230.67	5.17	230.89	5.39
O4	−64.09	−40.04	24.05	−38.26	25.83
O5	127.71	129.52	1.81	129.81	2.10

[a] For solvated systems, gas-to-solution shifts δ (in ppm) are also reported.

3.4. Nuclear Shielding. To complete the analysis of the solvent effects on the spectroscopic properties of GA, in this section, a study of the ^{17}O nuclear shielding in gas-phase, acetonitrile, and water is presented. Unfortunately, to the best of our knowledge, there are no experimental data to compare with. However, in our opinion, this study on NMR still can give interesting information on the effects of polar but aprotic and polar and protic solvents. This further analysis when compared with the previous IR and UV ones should in fact give a more complete picture of the solvation of GA.

As in the two previous analyses, also here we start by looking at the differences between isolated and IEFPCM solvated GA. In Table 4, ^{17}O nuclear shieldings are reported for GA in each phase together with solvent shifts $\delta = \sigma(\text{sol}) - \sigma(\text{vac})$ (in ppm). The results reported in Table 4 can be analyzed from different points of view.

First, the solvent shift is negative for O1 and O2 and positive for all of the other oxygens. This implies that the presence of a polar solvent leads to a deshielding for the internally H-bonded O and a shielding for all of the solvent-exposed oxygens. Let's try to better understand this point.

Nonspecific solvation as simulated by a continuum model like IEFPCM leads to a stronger diamagnetic shielding.[41] In fact, at the cavity surface, apparent charges are induced with opposite sign to those of the solute molecule. In this way, the

TABLE 5: B3LYP/6-311++G (GIAO) ^{17}O Nuclear Shieldings of the QM (1w,2w,8w) and MD Clusters (⟨*md*⟩), Possibly Including the IEF Continuum**

	VAC				IEF	
	1w	2w	8w	⟨*md*⟩	1w	2w
O1	232.69	233.10	218.54	223.92	231.20	231.97
O2	242.02	241.60	220.46	231.55	239.51	240.26
O3	226.29	226.54	214.34	216.49	230.32	230.69
O4	−41.77	−15.42	3.58	−16.43	−26.66	−19.06
O5	126.31	120.52	109.06	116.59	128.27	117.39

charges of the solute molecule are stabilized by Coulomb attraction; that is, the negatively charged O atoms become more negatively charged and therefore get a diamagnetic shift to higher field. This means a shielding effect and thus an increase of the net value of σ. This is exactly what is observed for the solvent-exposed O3, O4, and O5 (notice that for O4 the σ is negative and thus an increase of the diamagnetic part implies a less negative value). By contrast, for the internally H-bonded O1 and O2, the effect of the continuum is in the direction of decreasing the value of σ: in this case, such an effect can be explained looking at the changes in the H-bond lengths in Figure 6. The addition of the continuum in fact makes the internal H-bond longer (and weaker) and thus σ becomes closer to that of a free oxygen (i.e., O3).

The second observation to make about the results of Table 4 is that the carbonylic oxygen (O4) is the most sensitive to the environment: this is not surprising, because this oxygen is dominated by the paramagnetic part which is largely dependent on the environment.

Following the analysis of the previous sections, a better description of the solvent effects in the case of water, requires to include possible intermolecular hydrogen bonding effects by considering gallic acid−water clusters.

As done in the previous analysis of electronic transitions, also here solute−solvent clusters alternatively obtained through QM geometry optimizations and MD simulations are considered. The QM structures here considered are those reported in Figures 6 and 8, whereas the systems obtained from MD simulations are described in section 2.3. Once again, the results reported in Table 5 for MD-derived systems refer to a set of 10 clusters selected as described above and used to compute O nuclear shieldings without adding the IEF continuum. The computed shieldings of the different structures (which are not reported) of each set have been arithmetically averaged to give the values reported in Table 5 and marked as ⟨*md*⟩.

The comparison of the QM and MD clusters should give further hints on the nature of the solvation around GA, and in particular it should help in analyzing if these effects are better represented in terms of rigid structures obtained as the minima of the potential energy surfaces, or, on the contrary, if the real situation is dynamic and a variety of different and representative structures are to be considered.

As already noted above, a more direct analysis can be done in terms of solvent shift, defined as the difference between the oxygen shielding in the "model" solution (nw, nw+IEF, or ⟨*md*⟩) and in the isolated system. These data are reported in Figure 13. For a more direct analysis, in the same figures the values computed with the continuum only (IEF) are also reported.

The analysis of these graphs is articulate and thus we prefer to split it into parts, one focused on the small QM clusters (namely 1w and 2w) and the other on the larger MD clusters together with the QM 8w cluster.

The analysis on the small QM clusters (with or without the external continuum) is strictly connected with the previous one

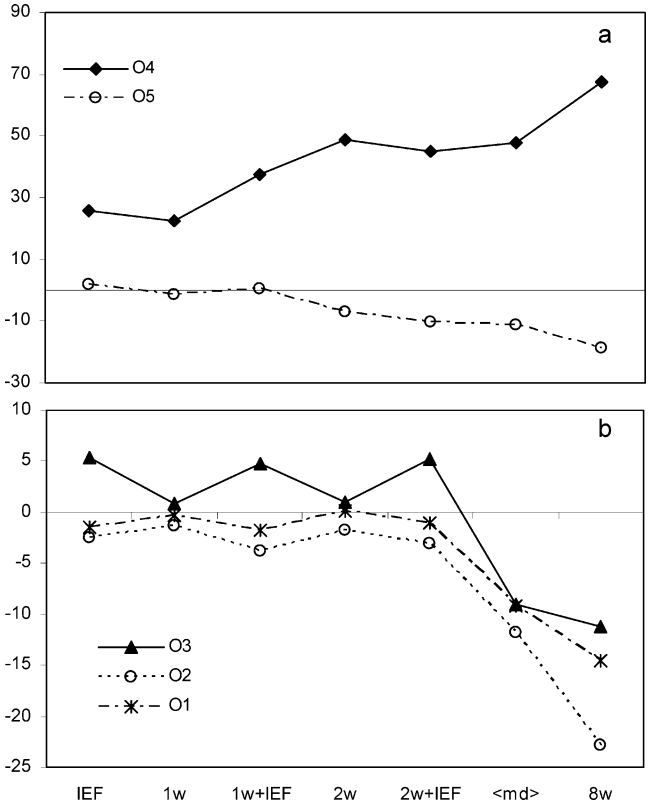

Figure 13. Solvent shift (ppm), defined as the difference between the oxygen shielding in the "model" solution (nw, nw+IEF, or ⟨*md*⟩) and in the isolated system for O4 and O5 nuclei (a) and for O1, O2 and O3 nuclei (b). For a more direct analysis, in the same figures values computed with the continuum only (IEF) are also reported.

done on the different solvent shifts induced by the continuum on the different nuclei. Also here, it appears evident the specificity of O4 with respect to all of the other oxygens. For O4, in fact, shifts ranging from 20 (with one water) to 50 ppm (with two water molecules) are observed, whereas for all of the others, the maximum shift is always less than 10 ppm for O5 and less than 5 ppm for O1−O3.

The effect of an explicit H-bonded water (1w) on the O4 nuclear shielding is very similar to that obtained without the explicit water but with the continuum (IEFPCM), i.e., a less negative σ: by combining the two effects (in 1w+IEF cluster), a double effect is not obtained (as it would be if the two were additive) but still a positive combination leading to a larger 37 ppm shift. The H-bonded water, as expected, does not significantly affect the other oxygens, and their nuclear shieldings σ remain very similar to the ones (in gas or with IEF) in the corresponding systems without the explicit water molecule. The second explicit water (in 2w and 2w+IEF clusters) is directly bonded to O5 (see Figure 6) and only indirectly affects O4 (in the case of 2w+IEF this indirect effect is expected to be even smaller due to the larger O4−HOH distance). As a result, one would expect that σ(O5) nuclear shielding changes significantly passing from 1w to 2w (or from 1w+IEF to 2w+IEF) but not σ(O4). This is not the case, as both oxygens are modified in a similar way by the second water: to explain this unexpected result, we have to resort to some kind of conjugation effects through the COOH moiety.

Another interesting result is that, for O5, the effects of an explicit H-bond and that of the continuum are opposite: the H-bond induces a deshielding (negative shift), whereas the continuum induces a shielding (positive shift) effect with the H-bond effect being stronger, because in the 2w+IEF a net

negative shift is observed. This opposite effect can be explained as follows. As said before, the continuum increases the negative charge at the O atom (and it decreases the electron density at H) and thus it induces a shielding effect. The same would be valid also for the electrostatic part of H bonding, but the covalent part leads, by contrast, to a delocalization of the O−H bonding pair over three centers and, accordingly, decreases diamagnetic shielding (and increases paramagnetic deshielding).

As expected, for O1, O2, and O3, the addition of one or two waters H-bonded to the carboxyl group does not induce important changes either in the gas-phase clusters or in the IEFPCM solvated ones.

Let us now pass to the second part of the analysis namely that on MD-derived clusters and the large QM 8w system.

The first thing to note is that, although the results obtained by averaging on different MD clusters are in line with the previous ones (even if with some differences which will be analyzed below), the 8w results are quite different from all of the rest especially for O4 and O5. Let us try to identify possible reasons by first looking at the MD results.

For both O4 and O5, the averaging over different clusters is almost identical to the combination of short-range H-bond effects and bulk effects: in fact, for both nuclei, the $\langle md \rangle$ shift is very similar to that obtained in the 2w+IEF model. Things are different for O1−O3 nuclei, where the $\langle md \rangle$ shift is significantly different from that obtained with any other QM cluster: this is easy to understand as the QM clusters do not involve any short-range intermolecular effects between hydroxyl groups and water molecules, whereas the MD clusters do include these effects. This is also confirmed by the 8w results which, for O3 (i.e., the nucleus not internally H-bonded), are very similar to the MD ones as this time the QM clusters include water molecules directly interacting with the O3H (see Figure 8). For the other two phenolic oxygens (O1 and O2) the agreement between $\langle md \rangle$ and 8w results is worse: this is due to the by far stronger H-bonding effects introduced in the QM 8w cluster than in the ones obtained from MD simulations. However, the largest discrepancies between $\langle md \rangle$ and 8w results are on O4 and O5. In the case of O4, the shielding effect of the water molecules in the 8w cluster is so strong to largely reduce the paramagnetic contribution, and as a result, the σ (O4) becomes positive (see Table 5). This large effect can be explained in terms of the overestimation of H-bonding effects, as already observed for UV spectra. Indeed in the 8w clusters there are two waters directly H-bonded to O5 and a third one indirectly linked through the O5H group.

A parallel strong but opposite effect is found on O5: here the presence of the waters directly H-bonded to O5 and to the linked hydrogen leads to a decrease of the net nuclear shielding σ (i.e., a deshielding effect) when compared to all of the other clusters.

4. Summary and Conclusions

In this paper, a study on the solvation of GA has been performed by means of its spectroscopic properties. Various solvation models obtained in terms of both purely classical and quantum-mechanical approaches have been used and compared.

The first step of the analysis has been the study of the minimum energy structures of GA. Using such a structure, an MD study has been performed, which has shown the different solvation of GA in water and in the aprotic acetonitrile. This MD analysis has been finally complemented with QM calculations on IR, UV, and NMR spectra of GA in water and in acetonitrile.

The comparison between experimental and calculated IR spectra of hydrated GA with different solvation models (continuum-only description or clusters obtained by adding one, two and eight explicit water molecules, possibly adding the external IEFPCM) shows that the inclusion of explicit solvent molecules affects the prediction of IR spectra more than the inclusion of averaged dielectric effects. In addition, the complete saturation of all possible H-bond sites of GA (in the cluster with eight waters) results in a better agreement between experimental and predicted spectra, whereas the simple inclusion of H-bond effects on the carboxyl groups does not lead to significative improvement in the quality of calculated spectra. This is not surprising if the nature of normal modes associated to bands in the range 1300−1500 cm^{-1} is considered, because they are due to complex motions mainly involving bending vibrations of the phenolic groups.

A parallel analysis has been performed on UV spectra both in water and in acetonitrile. Following the MD analysis, a continuum-only description has been used for the less selective acetonitrile, whereas for water clusters obtained by adding one, two and eight explicit water molecules (eventually adding the external IEFPCM) have also been considered, as well as clusters obtained from MD simulations. The results obtained with these latter clusters are in line with the values computed including both H-bond and bulk effects through QM clusters. This seems to indicate that most of solvent effect is of pure electrostatic origin, in fact the main part of the gas-to-water shift is recovered by the continuum-only description and the additional inclusion of explicit waters only results in a further small correction. It is interesting to note that the eight water cluster, which proved to give a correct picture for IR vibrations, in the case of UV gives a large red-shift which does not reproduce experimental findings. This shift seems to be due to an overestimation of solvent effects in this cluster.

This apparent contradiction between IR and UV results can be explained observing that the electronic transitions mainly involve the carbonyl moiety while IR vibrations for this part of the molecule cannot be compared to experiments. In fact, there is big noise in the region around water bending vibration (1640 cm^{-1}), and this noise hides the frequency region corresponding to the C═O stretching. IR and UV analyses can thus give only complementary information and, as a consequence, it is possible that the large 8w cluster properly describes solvation in the phenolic region while it overestimates H-bond effects on the carbonyl moiety.

For NMR shieldings, there are not available experimental data to compare with and thus it is not possible to discriminate among the different models by looking at the comparison between computed and measured shieldings. However, some conclusions can still be drawn. The first important observation is the very good agreement between MD clusters and the QM-IEF cluster with two water molecules on the carbonyl (IEF+2w) as far as the nuclear shieldings of O4 and O5 are concerned. This shows that, by combining a small solute−solvent cluster (which accounts for the most important specific and short-range interactions) with an embedding continuum (which accounts for the longest range bulk interactions) an accurate description can be obtained on solvation effects on a local property, i.e., the nuclear shielding of strongly H-bonded sites such as the COOH group in water. A parallel description on O1−O3 is not necessary because these sites are already partially "solvated" by internal H-bonds and thus the rest of solvation (the external contribution) can affect the net values in a much more limited way. It is also interesting to note that for all oxygens, the rigid

picture represented by the large QM 8w clusters seems to overestimate solvation effects. This means that, to represent a dynamic phenomenon such as solvation, careful attention has to be paid to the reliability of the simplified and static picture given by a single large solute−solvent cluster. In fact, effects of statistical averages have always to be taken into account either by referring to MD studies or, more simply, by introducing continuum descriptions, at least to properly account for the effects of the "nonbonding" part of solvent.

Acknowledgment. The UV spectra were measured by Dr. Lisa Ghezzi at the Department of Chemistry of the University of Pisa. The experimental IR spectra were kindly provided by Prof. Bernhard Lendl at the Institute of Chemical Technologies and Analytics of Vienna University of Technology.

Supporting Information Available: B3LYP/6-311++G** Cartesian coordinates of conformers A and B in gas-phase and in water (with the IEF continuum), A1w and A2w clusters in gas-phase and in water (with the IEF continuum), and A8w and B8w clusters in gas-phase. B3LYP/6-311++G** IR spectra of averaged conformers (A and B), A1w and A2w clusters in gas (VAC) and with the IEF continuum (water). This material is available free of charge via the Internet at http://pubs.acs.org.

References and Notes

(1) (a) Tang, H. R.; Covington, A. D.; Hancock, R. A. *Biopolymers* **2003**, *70*, 403. (b) Tang, H. R.; Covington, A. D.; Hancock, R. A. *J. Agric. Food Chem.* **2003**, *51*, 6652.

(2) Gomes, C. A.; Girão da Cruz, T.; Andrade, J. L.; Milhazes, N.; Borges, F.; Marques, M. P. M. *J. Med. Chem.* **2003**, *46*, 5395.

(3) Polewski, K.; Kniat, S.; Slawinska, D.*Curr. Top. Biophys.* **2002**, *26*, 217.

(4) (a) Zheng, W.; Wang, S. Y. *J. Agric. Food Chem.* **2001**, *49*, 5165. (b) Landrault, N.; Poucheret, P.; Ravel, P.; Gasc, F.; Cros, G.; Teissedre, P. L. *J. Agric Food Chem* **2001**, *49*, 3341. (c) Kahkonen, M. P.; Hopia, A. I.; Vuorela, H. J.; Rauha, J. P.; Pihlaja, K.; Kujala, T. S.; Heinonen, M. *J. Agric. Food Chem.* **1999**, *47*, 3954.

(5) (a) Serrano, A.; Palacios, C.; Roy, G.; Cespon, C.; Villar, M. L.; Nocito, M.; Gonzalez-Porque, P. *Arch. Biochem. Biophys.* **1998**, *350*, 49. (b) Silva, F. A. M.; Borges, F.; Ferreira, M. A. *J. Agric. Food Chem.* **2001** *49*, 3936.

(6) VanBesien, E.; Marques, M. P. M. *J. Mol. Struct. (THEOCHEM)* **2003**, *625*, 265.

(7) (a) Sroka, Z.; Rzadkowska-Bodalska, H.; Mazol, I. *Z. Naturforsch [C]* **1994**, *49*, 881. (b) Li, A. S.; Bandy, B.; Tsang, S. S.; Davison A. J. *Free Radical Res.* **2000**, *33*, 551.

(8) Dowd, P. F.; Duvick, J. P.; Rood, T. *Nat. Toxins* **1997**, *5*, 180.

(9) (a) Kerry, N. L.; Abbey, M. *Atherosclerosis* **1997**, *135*, 93. (b) Abella, A.; Chalas, J. *Atherosclerosis* **1997**, *134*, 199.

(10) Lu, Y.; Bennick, A. *Arch. Oral Biol.* **1998**, *43*, 717−728.

(11) Mitjavila, S.; Lacombe, C.; Carrera, G.; Darache, R. *J. Nutr.* **1977**, *107*, 2113.

(12) Nakamura, Y.; Torikai, K.; Ohto, Y.; Murakami, A.; Tanaka, T.; Ohigashi, H. *Carcinogenesis* **2000**, *21*, 1899.

(13) Madhan, B.; Thanikaivelan, P.; Subramanian, V.; Raghava Rao, J.; Nair, B. U.; Ramasami, T. *Chem. Phys. Lett.* **2001**, 346, 334.

(14) Bronco, S.; Cappelli, C.; Monti, S. *J. Phys. Chem. B* **2004**, *108*, 10101.

(15) Edelmann, A.; Lendl, B. *J. Am. Chem. Soc.* **2002**, *124*, 14741.

(16) (a) Sergediene, E.; Jonsson, K.; Szymusiak, H.; Tyrakowska, B.; Rietjens, I. C. M.; Cenas, N. *FEBS Lett.* **1999**, *462*, 392. (b) Castellucio, C.; Paganga, G.; Melikian, N.; Bolwell, G. P.; Pridham, J.; Sampson, J.; Rice, E. C. *FEBS Lett.* **1995**, *368*, 188. (c) Passi, S.; Picardo, M.; Nazarro-Porro, M. *Biochem. J.* **1987**, *245*, 537.

(17) (a) Tanaka, K.; Sakai, S.; Tomiyama, S.; Nishiyama, T.; Yamada, F. *Bull. Chem. Soc. Jpn.* **1991**, *64*, 2677. (b) Tomiyama, S.; Sakai, S.; Nishiyama, T.; Yamada, F. *Bull. Chem. Soc. Jpn.* **1993**, *66*, 299. (c) Vedernikova, I.; Proinov, E.; Salahub, D. R.; Haemers, A. *Int. J. Quantum Chem.* **1999**, *77*, 161. (d) Rajan, P.; Vedernikova, I.; Cos, P.; Vanden Berghe, O.; Augustyns, K.; Haemers, A. *Bioorg. Med. Chem. Lett.* **2001**, *11*, 215. (e) Bakalbassis, E.; Chatzopoulou, A.; Melissas, V. S.; Tsimidou, M.; Tsolaki, M.; Vafiadis, A. *Lipids* **2001**, *36*, 181.

(18) Mohammed-Ziegler, I.; Billes, F. *J. Mol. Struct. (THEOCHEM)* **2002**, *618*, 259.

(19) (a) Cancès, E.; Mennucci, B. *J. Math. Chem.* **1998**, *23*, 309. (b) Cancès, E.; Mennucci, B.; Tomasi, J. *J. Chem. Phys.* **1997**, *107*, 3031. (c) Mennucci, B.; Cancès, E.; Tomasi, J. *J. Phys. Chem. B* **1997**, *101*, 10506.

(20) (a) Miertus, S.; Scrocco, E.; Tomasi, J. *Chem. Phys.* **1981**, *55*, 117. (b) Cammi, R.; Tomasi, J. *J. Comput. Chem.* **1995**, *16*, 1449.

(21) Tomasi, J.; Cammi, R.; Mennucci, B.; Cappelli, C.; Corni, S. *Phys. Chem. Chem. Phys.* **2002**, *4*, 5697.

(22) Cappelli, C.; Mennucci, B.; da Silva, C. O.; Tomasi, J. *J. Chem. Phys.* **2000**, *112*, 5382.

(23) Mennucci, B. *J. Am. Chem. Soc.* **2002**, *124*, 1506.

(24) Cappelli, C.; Corni, S.; Mennucci, B.; Cammi, R.; Tomasi, J. *J. Phys. Chem. A* **2002**, *106*, 12331.

(25) Mennucci, B.; Martínez, J. M.; Tomasi, J. *J. Phys. Chem. A* **2001**, *105*, 7287.

(26) Frisch, M. J.; Trucks, G. W.; Schlegel, H. B.; Scuseria, G. E.; Robb, M. A.; Cheeseman, J. R.; Montgomery, J. A. Jr.; Vreven, T.; Kudin, K. N.; Burant, J. C.; Millam, J. M.; Iyengar, S. S.; Tomasi, J.; Barone, V.; Mennucci, B.; Cossi, M.; Scalmani, G.; Rega, N.; Petersson, G. A.; Nakatsuji, H.; Hada, M.; Ehara, M.; Toyota, K.; Fukuda, R.; Hasegawa, J.; Ishida, M.; Nakajima, T.; Honda, Y.; Kitao, O.; Nakai, H.; Klene, M.; Li, X.; Knox, J. E.; Hratchian, H. P.; Cross, J. B.; Adamo, C.; Jaramillo, J.; Gomperts, R.; Stratmann, R. E.; Yazyev, O.; Austin, A. J.; Cammi, R.; Pomelli, C.; Ochterski, J. W.; Ayala, P. Y.; Morokuma, K.; Voth, G. A.; Salvador, P.; Dannenberg, J. J.; Zakrzewski, V. G.; Dapprich, S.; Daniels, A. D.; Strain, M. C.; Farkas, O.; Malick, D. K.; Rabuck, A. D.; Raghavachari, K.; Foresman, J. B.; Ortiz, J. V.; Cui, Q.; Baboul, A. G.; Clifford, S.; Cioslowski, J.; Stefanov, B. B.; Liu, G.; Liashenko, A.; Piskorz, P.; Komaromi, I.; Martin, R. L.; Fox, D. J.; Keith, T.; Al-Laham, M. A.; Peng, C. Y.; Nanayakkara, A.; Challacombe, M.; Gill, P. M. W.; Johnson, B.; Chen, W.; Wong, M. W.; Gonzalez, C.; Pople, J. A. *Gaussian 03*, revision A.1; Gaussian, Inc.: Pittsburgh, PA, 2003.

(27) Tomasi, J.; Persico, M. *Chem. Rev.* **1994**, *94*, 2027.

(28) Cammi, R.; Cappelli, C.; Corni, S.; Tomasi, J. *J. Phys. Chem. A* **2000**, *104*, 9874.

(29) Mennucci, B.; Cammi, R.; Tomasi, J. *J. Chem. Phys.* **1998**, *109*, 2798.

(30) (a) Hameka, H. F. *Rev. Mod. Phys.* **1962**, *34*, 87. (b) Ditchfield, R. *Mol. Phys.* **1974**, *27*, 789. (c) Wolinski, K.; Hinton, J. F.; Pulay, P. *J. Am. Chem. Soc.* **1990**, *112*, 8251.

(31) (a) Cammi, R. *J. Chem. Phys.* **1998**, *109*, 3185. (b) Cammi, R.; Mennucci, B.; Tomasi, J. *J. Chem. Phys.* **1999**, *110*, 7627.

(32) (a) Simon, S.; Duran, M.; Dannenberg, J. J. *J. Chem. Phys.* **1996**, *105*, 11024. (b) Boys, S. F.; Bernardi, F. *Mol. Phys.* **1970**, *19*, 553.

(33) Halgren, T. A. *J. Comput. Chem.* **1996**, *17*, 490. (b) Halgren, T. A. *J. Comput. Chem.* **1996**, *17*, 520. (c) Halgren, T. A. *J. Comput. Chem.* **1996**, *17*, 553. (c) Halgren, T. A. *J. Comput. Chem.* **1996**, *17*, 616. (d) Halgren, T. A.; Nachbar, R. B. *J. Comput. Chem.* **1996**, *17*, 587.

(34) SYBYL Molecular Modelling Software, Version 6.9 (Linux OS2); TRIPOS Associates: St. Louis, MO, 2003.

(35) Case, D. A.; Pearlman, D. A.; Caldwell, J. W.; Cheatham, T. E., III; Wang, J.; Ross, W. S.; Simmerling, C. L.; Darden, T. A.; Merz, K. M.; Stanton, R. V.; Cheng, A. L.; Vincent, J. J.; Crouley, M.; Tsui, V.; Gohlke, H.; Radmer, R. J.; Duan, Y.; Pitera, J.; Massova, I.; Seibel, G. L.; Singh, U. C.; Weiner, P. K.; Kollman, P. A. AMBER 7; University of California: San Francisco, 2002.

(36) Jorgensen, W. L. *J. Am. Chem. Soc.* **1981**, *103*, 335.

(37) Grabuleda, X.; Jaime, C.; Kollman, P. A. *J. Comput. Chem.* **2000**, *21*, 901.

(38) (a) Cieplak, P.; Cornell, W. D.; Bayly, C. I.; Kollman, P. A. *J. Comput. Chem.* **1995**, *6*, 1357. (b) Bayly, C. I.; Cieplak, P.; Cornell, W. D.; Kollman, P. A. *J. Phys. Chem.* **1993**, *97*, 10269.

(39) Berendsen, H. J. C.; Postma, J. P. M.; vanGunsteren, W. F.; DiNola, A.; Haak, J. R. *J. Comput. Phys.* **1984**, *81*, 3684.

(40) UV spectra (1.4×10^{-5} M) were measured by Dr. Lisa Ghezzi at the Department of Chemistry of the University of Pisa using the Perkin-Elmer Lambda 6 UV−vis spectrometer at pH = 4.5 and 1.91.

(41) Wu, A. A.; Cremer, D.; Gauss, J. *J. Phys. Chem. A* **2003**, *107*, 8737.